Chirality | WILEY

Chiral voltammetric sensor for tryptophan enantiomers by using a self-assembled multiwalled carbon nanotubes/polyaniline/sodium alginate composite

Xiaohui Niu[1] | Xing Yang[2] | Hongxia Li[1] | Qiuyun Shi[1] | Kunjie Wang[1] 🟢

[1]College of Petrochemical Technology, Lanzhou University of Technology, Lanzhou, China

[2]College of Polymer Science and Engineering, State Key Laboratory of Polymer Materials Engineering, Sichuan University, Chengdu, China

Correspondence
Kunjie Wang, College of Petrochemical Technology, Lanzhou University of Technology, Lanzhou, China.
Email: wangkj80@163.com

Abstract

Due to the crucial role of amino acids in life sciences and pharmaceutics, identification of optical amino acid molecules is of great significance. In this study, the two materials (CNT and PANI) were combined together to obtain the magnification of electrochemical signal by substrate material (CNT/PANI). Then a self-assembled multiwalled carbon nanotubes/polyaniline/sodium alginate (CNT/PANI/SA) nanocomposite with chiral sites and conductive material was synthesized as the electrochemical sensing interface. Next, a novel electrochemical sensing interface was fabricated via modifying the as-prepared chiral material on a polished glassy carbon electrode (CNT/PANI/SA/GCE) for precisely, efficiently, and rapidly differentiation of tryptophan (Trp) enantiomers. It was observed that CNT/PANI/SA/GCE showed desirable stereoselective recognition effect in the variety of signal strength to peak current (Ip) to the different optical activity of Trp enantiomers. In the case of optimal conditions, the peak current ratio in the solution of L-Trp and D-Trp (I_D/I_L) was observed to be 2.1 at CNT/PANI/SA/GCE by differential pulse voltammogram (DPV). UV–visible spectroscopy further showed that CNT/PANI/SA had a greater binding energy to L-Trp. Also different factors affecting the enantioselectivity of CNT/PANI/SA/GCE, such as the incubation time, pH, and dropcoating volume of CNT/PANI/SA were optimized. Moreover, the proposed CNT/PANI/SA/GCE showed excellent specific stereoselectivity and anti-interference ability. Besides, the proposed chiral sensing platform can be effectively applied in real samples to detect Trp enantiomers sensitively. This work inspires us a new path for the preparation of substrate material with excellent electrical conductivity, as well as extend its application potential in chiral recognition.

KEYWORDS
chiral composite, electrochemical sensing interface, molecule recognition, self-assembly, sodium alginate

1 | INTRODUCTION

With the development of chiral separation in biology, researchers have updated many conventional ideas. Take amino acids as an example, the majority of D-configuration amino acids have been found in mammals and humans, which has subverted the concept that D-configuration amino acids only can be synthesized.[1] However, a large number of studies have proved that only L-configuration amino acids have favorable impact, and the corresponding D-configuration may be invalid or even produce irreversible side effects.[2] Therefore, chiral discrimination is a key problem in analytical chemistry. At present, many techniques have been exploited to efficiently, rapidly and sensitively distinguish chiral amino acids. Unfortunately, most of the traditional technologies have some limitations. Circular dichroism (CD) exhibits low sensitivity. Instrumental analysis has high requirements for equipment and high price.[3] Surface-enhanced Raman scattering is subjective to the substrates.[4] Fluorescence analysis is very sensitive to intrusion originating from other unrelated molecules, thus causing the variation in fluorescence intensity.[5] These methods are troublesome and expensive for chiral recognition.

Alternatively, the electrochemical measurement is of significance due to the advantages of fast detection, low prices, high sensitivity, and anti-jamming property.[6–8] Many scholars made great effort on the investigation of chiral selectors used for the fabrication of electrochemical sensing interface, such as chiral carbon dots, amino acid, chiral supramolecules, and MOFs.[9–12] In some cases, only modifying the chiral selectors on the electrode will hinder electronic transmission of chiral interface, weakening chiral recognition signal. Therefore, it is still necessary to develop an efficient electrochemical chiral sensing interface in the detection of optically active molecules.

Natural polysaccharides with definite structure and chiral properties, such as cellulose and its derivatives, chitosan and its derivatives are the biopolymers existed in large amount. Since the optical activity of polysaccharides was certified by Kotake et al.,[13] polysaccharides and their derivatives as chiral selectors have been widely applied in stationary phases for separation optically active molecules.[14] Sodium alginate (SA), a by-product extracted from seaweed or Sargassum, is chiral molecule with excellent biocompatible, film-forming, and nontoxic properties. SA-based materials have been widely applied in food science. In recent years, the extensive application was developed for chiral recognition of tyrosine enantiomers via chiral ligand exchange principle, indicating the chiral properties of SA made it as a choice in electrochemical chiral sensing interface.[15] Therefore, SA has application potential in the construction of electrochemical chiral sensors due to its biocompatible and film-forming. Moreover, given its chiral characteristics and coordination ability, it has aroused widespread interest to use SA as a chiral ligand to apply in chiral ligand exchange principle for chiral separation purpose.[16] However, due to the insulating properties of polysaccharides, the application of polysaccharides is limited in the construction of electrochemical sensing interfaces. In recent years, the integration of polysaccharide science with electrochemical technology for electrochemical recognition of optically active molecules was studied by our previous report, such as β-cyclodextrin,[17] self-assembled polysaccharide,[18] and CS.[19] Unfortunately, the expected electrochemical signal was not obtained, which is probably due to the inferior conductivity and obvious aggregation of polysaccharides when they exist alone. Conductive polymer as a noticeable substrate material has attracted much attention due to its excellent electrochemical performance.[20] Polyaniline (PANI) has been regarded as one of conspicuous conductive polymer among electrode materials due to its excellent electrical conductivity and easy synthesis. Besides, chiral polyaniline can also be used in enantioselective separation.[21] However, in the process of the insertion/de-insertion of the counter-ions, the swelling/shrinkage of PANI will bring about volume changes and damage the backbone of PANI, which severely reduces the life of the electrode material, thereby hindering its application in electrochemistry field.[22] The integration of PANI with carbon nanotubes (CNT) has been shown to be appealing for enhancing the reliability of polyaniline and maximizing its electrical conductivity.[23]

In this context, a new self-assembled chiral multiwalled carbon nanotubes/polyaniline/sodium (CNT/PANI/SA) composite was combined as chiral materials for efficiently and highly selective recognition of L-Trp and D-Trp based on the differential pulse voltammetry measurement. This self-assembled one-pot reaction does not require one-pot reduction at a higher temperature, and the synthesized materials are more controllable. Once SA and CNT/PANI was united together, this chiral composite (CNT/PANI/SA) simultaneously synergizes the inherent chiral characteristics of SA as the chiral selector and the fast electronic transmission of CNT/PANI. Moreover, the introduction of SA in CNT/PANI may enhance the solubility of CNT/PANI, and CNT/PANI in SA can increase the electrochemical property of SA, which obtained the result of 1 + 1 > 2. Trp enantiomers were distinguished referred to different electrochemical signals based on the difference in affinity employing DPV. The enantioselectivity, reproducibility, and selectivity of the chiral sensing platform were also discussed. Finally, the ordered self-assembly CNT/PANI/SA nanocomposite was applied to determine L-Trp and D-Trp in actual samples.

2 | MATERIALS AND METHODS

Carbon nanotubes (CNT), ammonium persulfate (APS), L-tryptophan (L-Trp), and D-tryptophan (D-Trp) were obtained from Aladdin Chemistry Co., Ltd. Sodium alginate was purchased from Shanghai Macklin Biochemical Technology Co., Ltd. Aniline was from Sinopharm Chemical Reagent Co., Ltd. All chemical reagents were analytical grade. All solutions were prepared with deionized water (Milli-Q, Millipore); 0.1-M phosphate buffered saline (PBS) at different pH was obtained via mixing different amounts of 0.1-M KH_2PO_4 and 0.1-M K_2HPO_4 containing 0.1-M KCl.

2.1 | Apparatus

All of the electrochemical experiments were performed on a CHI660E electrochemical workstation (Shanghai Chen Hua Instruments Co., Ltd., China). Surface morphological studies of composites were examined were measured by scanning electron microscopy (SEM, ULTRA plus, Germany). EQUINOX-55 FTIR spectrometer (Shimadzu, Japan) was applied to obtain Fourier transform infrared (FT-IR) spectra of the composites over 4000–400 cm^{-1}. We performed X-ray diffraction (XRD) measurements with Cu Kα X-ray sources on a D/Max-2400 powder diffractometer (Japanese Physical Company). Ultraviolet–visible (UV–Vis) spectroscopy measurements were obtained from a UV-2550 spectrophotometer (Shimadzu, Japan).

2.2 | Synthesis of chiral CNT/PANI/SA composite

The synthetic steps of CNT/PANI/SA nanocomposite were as follows: 0.04-g CNT were dispersed homogeneously in 30 ml of H_2O via ultrasound for 2 h. Then 3 mg ml^{-1} SA (20 ml, solvent: H_2O) and 10 ml of 0.25-M aniline monomers in 1-M HCl were mixed into CNT dispersion and sonicated for 40 min. Following, 20 ml of 0.25-M APS solution was quickly poured into the above-mentioned suspension and then reacted for 4.5 h. The CNT/PANI/SA composite was obtained by filtration via using 0.2-µm filter membrane. The synthesized CNT/PANI/SA composite was dried in vacuum dryer at 40°C for 12 h. For comparison, pure polyaniline and CNT/PANI were also prepared under the above-mentioned processes.

2.3 | Construction of the working electrode

Prior to construction of CNT/PANI/SA/GCE, CNT/PANI/GCE, and SA/GCE, the surface of glassy carbon electrode was polished with α-Al_2O_3 slurry (1.0 mm and 0.3 mm) until obtained a mirror plane. Then the polished electrode was sonicated in deionized water and ethanol sequentially, following dried under the infrared light. Subsequently, 1 mg of CNT/PANI/SA was scattered in 1-ml deionized water. Then the obtained suspension was sonicated for 30 min until obtained a uniform dispersion. Finally, 8 µl of dispersion was then drop-coating on the bare GCE and dried on infrared lamp, which was expressed as CNT/PANI/SA/GCE. CNT/PANI/GCE and SA/GCE were obtained with similar approach.

3 | RESULTS AND DISCUSSION

3.1 | Mechanism of the formation of chiral material

The formation mechanism of CNT/PANI/SA and CNT/PANI materials is shown in Scheme 1. The CNT
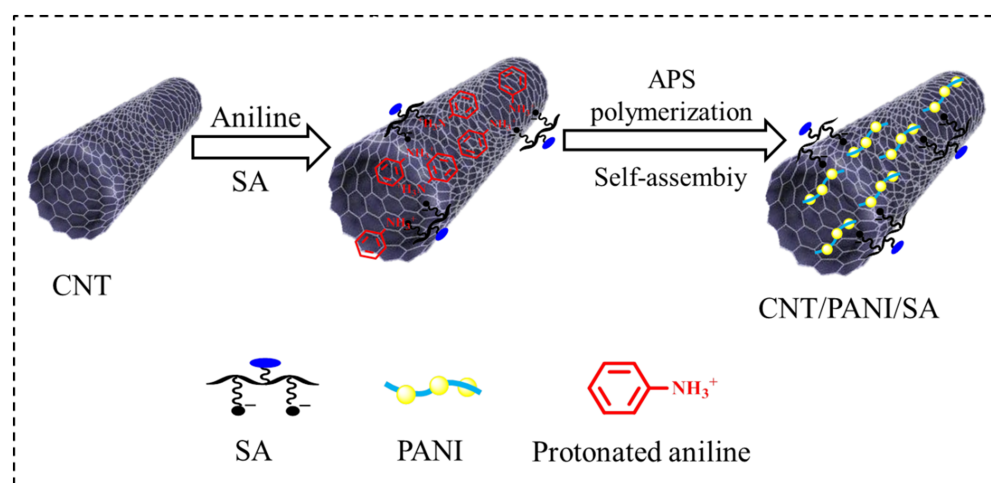
SCHEME 1 Synthesis of CNT/PANI/SA material

can be considered as electron acceptor and the protonated aniline monomer used as electron donor to obtain weak charge transport complexes. The protonated aniline monomer quickly can adsorb on the CNT immediately because of electrostatic interaction. PANI will form worm-like structure during polymerization in the absent of CNT. Conversely, CNT as a support material could serve as nucleation sites for PANI nucleation, and PANI particles can be anchored on the CNT surface, thus enhancing both the dispersion of PANI particles and the interaction of substrate material with solution, which may be beneficial to the amplification of the electrochemical signal as a substrate material.

The in situ oxidative polymerization of CNT/PANI/SA composites was carried out by one-pot synthesis method. Owing to SA will hydrolyze in acidic system, SA can dissolve in water. Therefore, the low-concentration hydrochloric acid solution of aniline monomer is immediately added to the SA solution. The introduction of HCl in the SA solution will facilitate the hydrolysis of the neutral $-COONa$ to the charged $-COO^-$. Then the negatively charged $-COO^-$ of SA will adsorb on the protonated
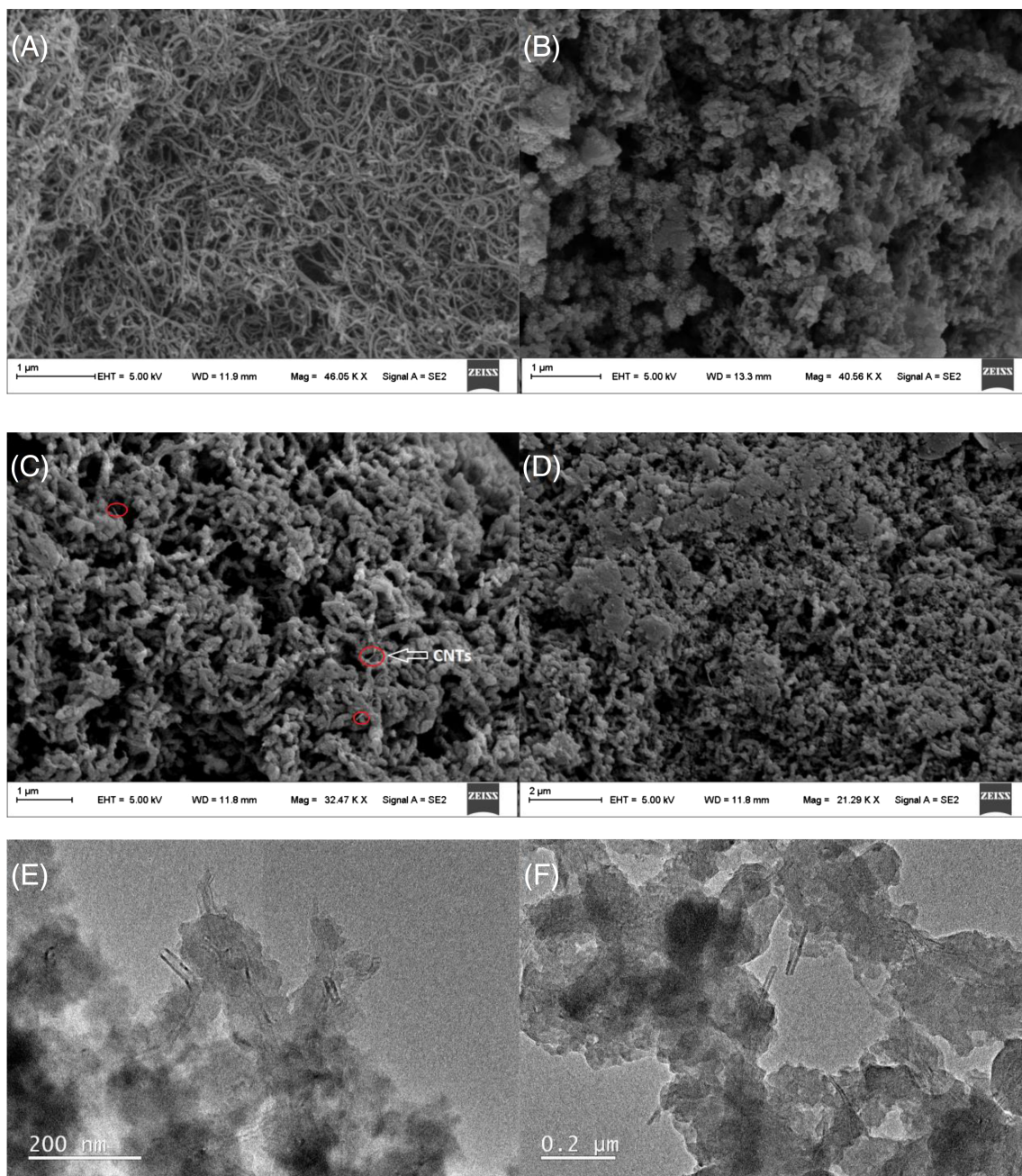

FIGURE 1 SEM image of pure CNT (A), PANI (B), CNT/PANI (C), and CNT/PANI/SA (D). TEM image of CNT/PANI (E) and CNT/PANI/SA composite (F)

amino of anline monomer through electrostatic attraction and formed complexes.[24] This process will not only maintain the structural integrity of SA during the hydrolysis process but also accelerate the decomposition of −COONa into −COO⁻. Moreover, many studies have shown that the conductivity of PANI synthesized under acidic conditions is better than that of PANI synthesized under alkaline or neutral conditions.[25] Simultaneously, aniline monomers can be combined on the surfaces of CNT immediately. In the synthesis process, CNT and SA can be considered as an electron-accepting while aniline was an electron-donating. During in situ polymerization, the synergistic effects between two pairs of electrostatic interactions promoted to the "re-growth" of the composite. Finally, the CNT/PANI/SA composite was thus synthesized.

3.2 | Characterizations

SEM and TEM measurements were performed to investigate the structures and morphologies of the various materials. Figure 1A exhibits the intertwined CNT with a tubular structure. As observed from Figure 1B, PANI particles will form worm-like structure during polymerization in absence of CNT. Once CNT is introduced during the process of polymerization, it can be observed that CNT was covered by PANI, showing that there has interaction between CNT and PANI. This interaction can reduce the π-π interaction between CNT, which usually leads to CNT agglomeration. As displayed in Figure 1E, the CNT/PANI composite with three dimensional structure can be seen clearly on the substrate. This result is the same as that of SEM measurement, showing in Figure 1C. Figure 1E exhibits that PANI particles anchored on the surface of CNT and linked by CNT

because of its large surface area and excellent chemical activity. As shown in Figure 1D,F, the three-dimensional structure of the CNT/PANI/SA is preserved even after the introduction of SA.

The SA, PANI, CNT/PANI, and CNT/PANI/SA were characterized by FT-IR (Figure 2A). The peak that appeared at 3446 cm⁻¹ of CMC is attributable to the stretching vibrations of OH. The typical peaks at 2976 and 2814 cm⁻¹ belong to stretching vibrations of aliphatic C–H. The characteristic peaks at 1630 and 1417 cm⁻¹ are due to asymmetric and symmetric stretching vibrations the carboxylate group (–COO⁻). The peak at 1043 cm⁻¹ is ascribed to stretching vibrations of C–O–C. It can be observed that the typical peaks of PANI appeared at 1562 cm⁻¹ and 1478 cm⁻¹, which are attributable to the stretching deformation of C=C in quinoid and benzene rings, respectively. The typical peaks that appeared at 1296 and 1248 cm⁻¹ are ascribed to stretching vibrations of C–N and C=N in aromatic amine, and the peaks at 1128 and 780 cm⁻1 are ascribed to the in-plane and out-of-plane bending vibration of C–H, respectively.[26] The characteristic peaks of CNT/PANI composite display the typical peaks similar to PANI. However, the C=C of quinonoid rings (1562 cm⁻¹) and benzenoid rings (1478 cm⁻¹) increase in the FT-IR spectra of CNT/PANI compared with the PANI. The enhanced "electronic-like peak" at 1128 cm⁻¹ related to the conductivity of PANI,[27] which is ascribed to π-π interaction between CNT and the PANI. CNT/PANI/SA composite has typical peaks both appeared at CNT/PANI and SA. The peaks of CNT/PANI at 1562 and 1478 cm⁻¹ are attributed to C=C in quinonoid rings and benzene rings. The peaks at 2976 and 2814 cm⁻¹ are stretching vibrations of aliphatic C–H, and the weak peaks at 1630 cm⁻¹ are to stretching vibrations of carbonyl in SA. All these results indicated that SA was anchored onto the CNT/PANI.
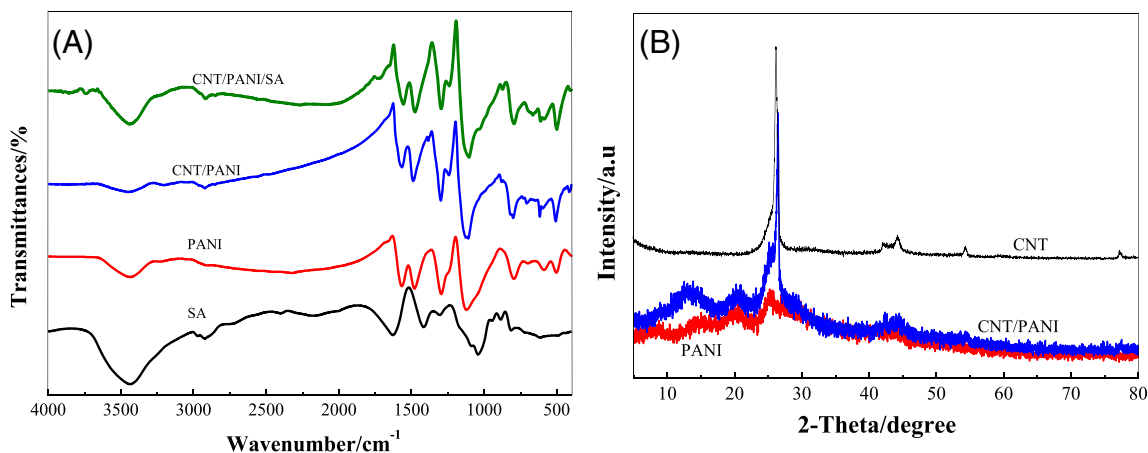

FIGURE 2 (A) FT-IR spectra of SA, pure PANI, and CNT/PANI and CNT/PANI/SA. (B) XRD patterns of CNT, pure PANI, and CNT/PANI composites

The XRD patterns of pure CNT, PANI, and CNT/PANI composites are shown in Figure 2B. For CNT, the typical characteristic peaks that appeared at $2\theta = 25.78°$ and $42.27°$ can be attributable to (002) and (100) diffraction peak of the graphite-like structure, respectively. For the XRD patterns of pure PANI, its typical crystalline peaks appear at $2\theta = 15.2°$, $20.0°$, and $25.1°$, which are ascribed to (011), (020), and (200) crystal planes of PANI in its emeraldine salt form, respectively.[28] The diffraction peak of CNT/PANI composite displays the typical characteristic peaks similar to those data observed on pure PANI, indicating that no other crystalline structure has appeared in the composites.

3.3 | Electrochemical characterizations

Cyclic voltammograms (CVs) were conducted to record the electrochemical recognition ability of various sensing interface (SA/GCE, CNT/PANI/GCE, and CNT/PANI/SA/GCE) by using 5.0-mM $[Fe(CN)_6]^{3-}$ and $[Fe(CN)_6]^{4-}$ as the redox probe in a 0.1-M KCl. It can be seen from Figure 3A that a reversible redox peak appears at bare GCE in 5-mM $[Fe(CN)_6]^{3-/4-}$ with a peak-to-peak separation in a potential (ΔEp) of 88 mV. A smaller peak current can be observed at SA/GCE (33.14 μA), which even lower than the peak current of bare electrode (43.18 μA) due to its insulation. However, the electrochemical signals of CNT/PANI/SA/GCE (70.41 μA) and CNT/PANI/GCE (134.06 μA) amplify successively. The results show that the integration of CNT and PANI can be used as substrate materials, facilitating electron transmission between chiral sensing interface and solution. Moreover, CNT/PANI/GCE shows the best electrochemical signal, revealing that CNT/PANI/GCE has highest electrical conductivity for the synergy of CNT and PANI. CNT/PANI possesses particular 3D microstructure to improve the effective area of working electrode, thus showing an excellent electrochemical activity to amplify the electrochemical signal of chiral sensing interface. The introduction of PANI particles further improve the conductivity of the base material and form sensing platform for Trp enantiomers. However, when SA was introduced in PANI/CNT composite, the peak-to-peak separation in a potential increases to 90 mV with a decline of electrochemical signal, showing that SA possesses inferior electrical conductivity.

Electrochemical impedance spectroscopy (EIS) was used to study the electrochemical impedance data at electrode and solution interfaces of different materials. The Nyquist diagram analysis also shows the modification of chiral composite is effective and feasible (Figure 3B). The semicircle and the approximate straight line of the Nyquist diagram corresponded to the high frequency region and the low frequency region, respectively. The Equivalent circuit diagram can be obtained from ZSimpWin software. It can be observed that the electron transfer resistance (Rct) data of PANI/GCE and CNT/PANI/GCE (201.12 Ω) is too small to be considered due to its excellent electrochemical performance. However, when compared with Rct data of SA/GCE (8826.21 Ω) and CNT/PANI/SA/GCE (3302.06 Ω), SA/GCE shows a bigger Rct than CNT/PANI/SA/GCE, indicating that the introduction of SA can decrease the electronic transmission of electrochemical interface. The results demonstrate that SA was anchored on the CNT/PANI successfully, which can be applied to construct the electrochemical chiral sensing interface and used to enantiorecognition of Trp enantiomers. The Nyquist diagram analysis is consistent with CV measurement and further proved the successful construction of CNT/PANI/SA-based composite electrochemical sensor.

The effect of scan rate on peak current was performed by CV measurement to explore the kinetic mechanism in working electrode reaction. As shown in Figure 3C, due to the resistance existed in CNT/PANI/SA/GCE, the anodic peak moves to negative potential and the cathodic peak changes to positive potential can be observed at the scan rates range from 10 to 110 mV s^{-1}.[29] It can be seen from Figure 3D that the sweep speed is proportional to the peak current, revealing that the electrochemical process was adsorption-controlled. The linear relationship can expressed to $I_{pa} = 0.95\nu + 20.67$ ($R^2 = 0.995$) and $I_{pc} = -0.73\nu - 18.26$ ($R^2 = 0.997$).

To evaluate the stability of CNT/PANI/SA/GCE sensing platform, CNT/PANI/SA/GCE was stored in the refrigerator for 10, 12, 14 16, 18, 20, and 22 days; its peak current was measured by CV. Then its stability was evaluated by the change of peak current. It can be seen from the Figure 3E that after 22 days of storage in the refrigerator, the peak current is only 3.4% less than the initial current, showing the stability of the sensing platform.

3.4 | Feasibility of electrochemical enantiorecognition based on CNT/PANI/SA/GCE

Electrochemical stereoselective recognition L-Trp and D-Trp at the CNT/PANI/SA-based chiral sensing interfaces was investigated. Additionally, control experiments were performed at the SA/GCE and PANI/SA/GCE. Figure 4 exhibits the difference in differential pulse voltammograms (DPVs) of L-Trp and D-Trp at various electrochemical sensing interfaces. According to previous reports, the DPV of L-Trp and D-Trp showed completely
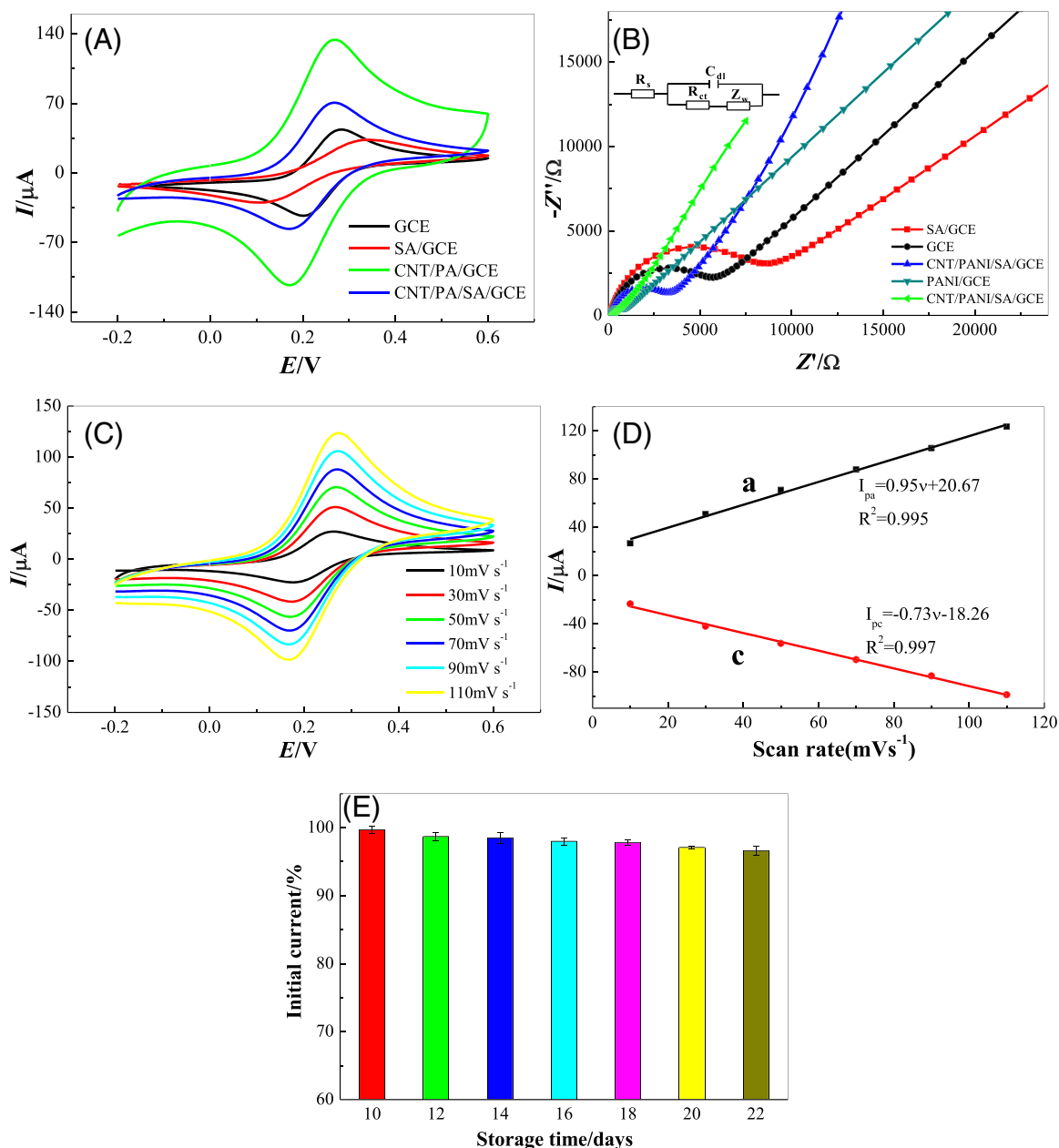
FIGURE 3 (A) CVs and (B) EIS obtained at bare GCE, SA/GCE, CNT/PANI/GCE, and CNT/PANI/SA/GCE in a 0.1-M KCl solution containing 5.0-mM $[Fe(CN)_6]^{3-}$ and $[Fe(CN)_6]^{4-}$. (C) CVs of CNT/PANI/SA/GCE at the scan rates of 10, 30, 50, 70, 90, and 110 mV s^{-1}. (D) Linear relationship of anodic and cathodic peaks with scan rate. (E) The stability of the CNT/PANI/SA/GCE

overlapped peak current on unmodified GCE, indicating that the bare GCE was incapable of identifying L-Trp and D-Trp due to the absent of chiral centers.[30] As shown in Figure 4A, the DPV of Trp isomers shows apparent differences in SA-modified GCE peak currents (Ip), whose efficient chiral recognition at SA/GCE might be attributable to the inherent chirality of SA. However, compared with CNT/PANI/SA/GCE, the small peak current ratio ($I_D/I_L = 1.9$) suggests that the recognition ability of pure SA does not match up to its promise. The inferior chiral recognition on SA/GCE can be explained by the fact that

SA is insulating when the lack of substrate materials, which result in weak electrochemical signal and low recognition efficiency when the interaction occurred between chiral host molecules (individual polysaccharide) and the recognized molecules (L-Trp and D-Trp) in the chiral interface based on SA. It can be seen that the DPVs of the CNT/PANI/GCE (Figure 4B) show no differences in the I_D/I_L (1.1). Therefore, the CNT/PANI/GCE exhibited no recognition ability towards Trp enantiomers. It is exciting to find that the I_D/I_L (2.1) is significantly increased at the CNT/PANI/SA modified
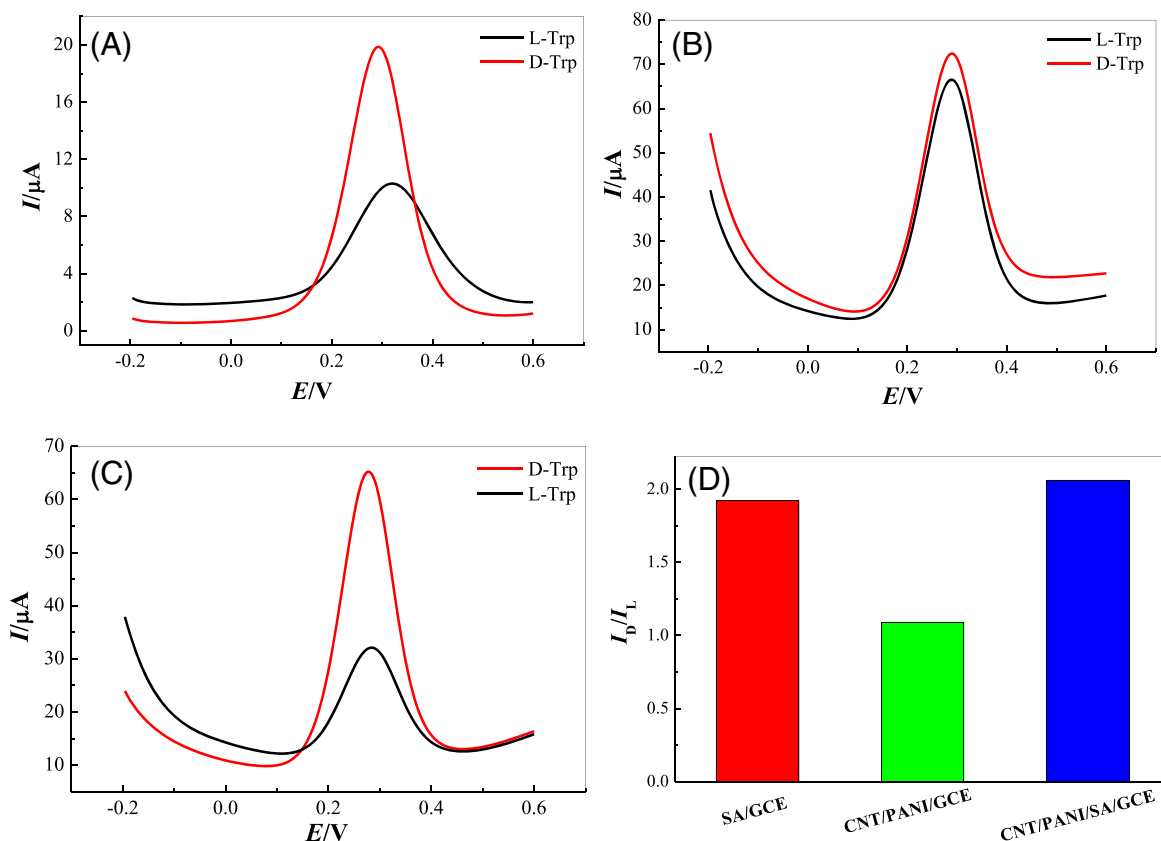
FIGURE 4 DPVs of 5-mM L-Trp and D-Trp included with SA/GCE (A), CNT/PANI/GCE (B), and CNT/PANI/SA/GCE (C). The peak current ratios (I_D/I_L) of different electrodes (D)

GCE (Figure 4C). The improved recognition efficiency at the CNT/PANI/SA-based chiral sensor might originate from the synergy of the excellent conductivity of CNT/PANI and the chiral properties of the SA, both of which are favorable to chiral recognition of L-Trp and D-Trp in chiral sensing interface based on CNT/PANI/SA. It can be seen from Figure 4C that CNT/PANI/SA/GCE has a smaller DPV peak current in L-Trp solution containing 5.0-mM $[Fe(CN)_6]^{4-/3-}$ at the potential range of −0.2 to 0.6 V, which shows that CNT/PANI/SA/GCE surface is combined with more L-Trp, resulting in a smaller peak current due to the insulation of L-Trp. The more L-Trp that CNT/PANI/SA/GCE binds, the greater the force on L-Trp. The greater effect of CNT/PANI/SA on L-Trp is because the hydroxyl group of CNT/PANI/SA and the amino group of L-Trp are more likely to form hydrogen bonds. Due to steric hindrance, the hydroxyl group of CNT/PANI/SA and the amino group of D-Trp cannot form a hydrogen bond. The carboxyl groups on L-Trp and D-Trp cannot easily form hydrogen bonds with the host due to the long distance. That is, when the chiral selector and the guest molecule form diastereoisomeric enantiomer-selector complexes through three-point forces, L-Trp has a greater force due to steric hindrance,

which allow more L-Trp molecules to remain on the electrode surface, resulting in a smaller peak current. The peak current ratios (I_D/I_L) of different electrodes are shown in Figure 4D.

UV–Vis spectroscopy were applied to record the absorbance of 0.2-mM L-Trp and D-Trp at a serious of concentrations of the CNT/PANI/SA ranging from 0.1 to 0.8 mM, which is to further study the binding thermodynamics during the enantioselective recognition of L-Trp and D-Trp. As shown in Figure 5A,B, the typical characteristic absorption peak of Trp at 279 nm gradually improved with the amplification of the CNT/PANI/SA concentration. The binding constant and stoichiometry ratio between CNT/PANI/SA and Trp isomers are obtained from the previous reported Equation 1[31]:

$$\frac{1}{A-A_0} = \frac{1}{\Delta\varepsilon \times [C_{Trp}]} + \frac{1}{(\Delta\varepsilon \times [C_{Trp}] \times K \times [CNT/PANI/SA]_0^n)}$$
(1)

Herein, A and A_0 represent the absorbance of L-Trp and D-Trp at every different concentrations of CNT/PANI/SA and in the absence of CNT/PANI/SA, respectively. $[CNT/PANI/SA]_0^n$ and $[C_{Trp}]$ are the concentrations of
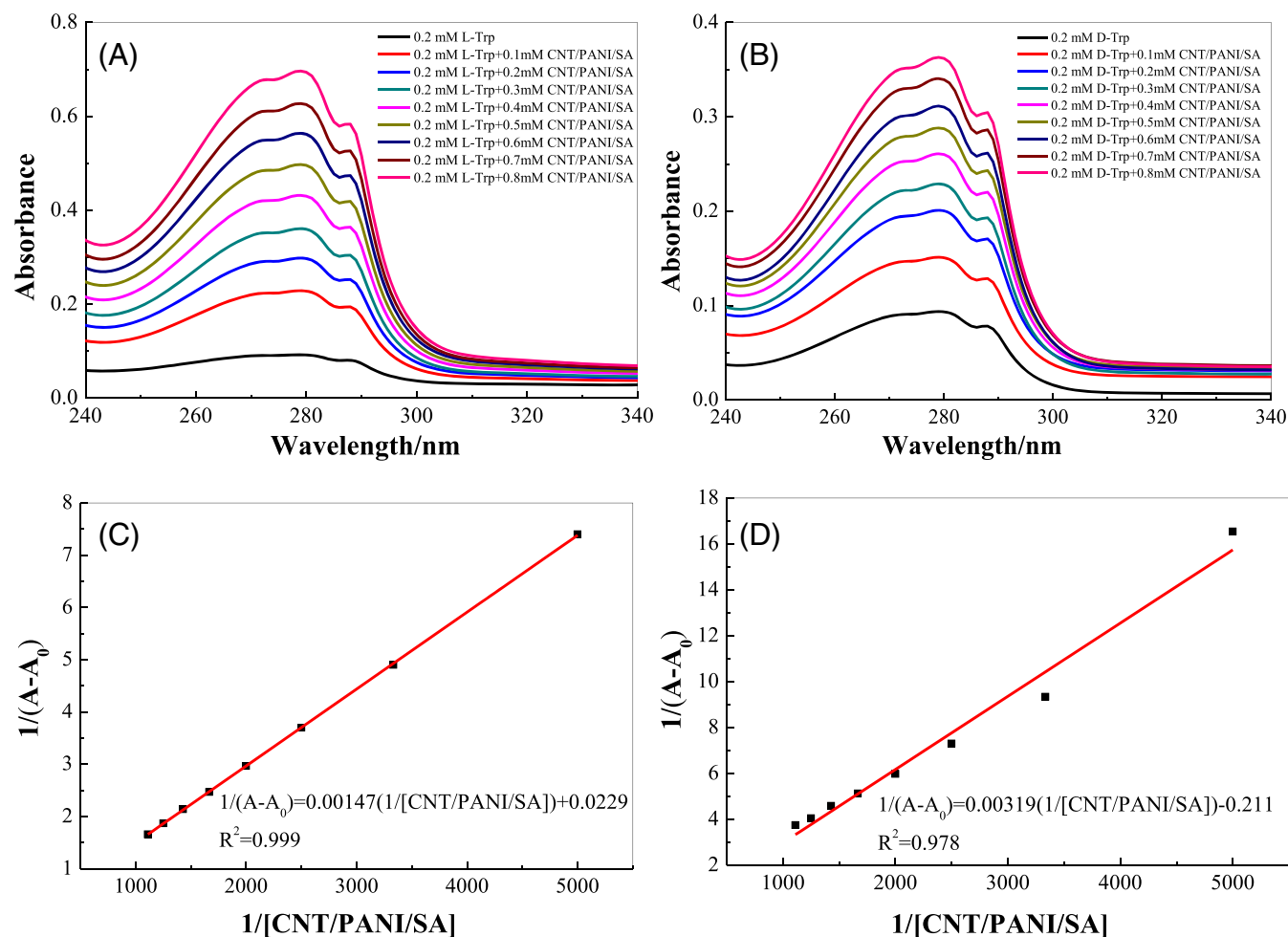
FIGURE 5 UV–Vis spectroscopy of 0.2-mM L-Trp (A) and D-Trp (B) after introduction of CNT/PANI/SA at a serious of concentrations. Double reciprocal linear relationships of L-Trp (C) and D-Trp (D) contained CNT/PANI/SA (pH = 6)

CNT/PANI/SA and L-Trp or D-Trp. The differential molar extinction coefficient of L-Trp as well as D-Trp in the presence and lack of CNT/PANI/SA is denoted as $\Delta\varepsilon$. n represents the stoichiometric ratio. Only when n equals stoichiometry ratio, a linear relationship can be obtained. The K value is obtained by the linear relationship of the double reciprocal plot, which can be calculated through dividing the intercept by the slope of the fitted line. The linear relationships of double reciprocal graph are shown in Figure 5C,D. The result showed the chiral sensing platform is efficient and feasible for stereoselective recognition of Trp isomers.

As illustrated in Figure 6, there has difference in the electrochemical responses of the chiral sensing interface to D-amino acids and L-amino acids. The specific stereoselectivity of CNT/PANI/SA/GCE for the Phenylalanine (Phe) enantiomers, Mandelic acid (MA) enantiomers, and Lysine (Lys) enantiomers was investigated. As displayed in Figure 6A–C, no obvious electrochemical response toward Lys at CNT/PANI/SA/GCE can be obtained. Obviously, CNT/PANI/SA/GCE exhibits better

recognition efficiency for Phe and MA due to the relatively stronger steric hindrance between CNT/PANI/SA/GCE and enantiomers. It can be observed that the CNT/PANI/SA/GCE exhibits specific stereoselectivity for L-Trp and D-Trp for the strongest steric hindrance between CNT/PANI/SA and Trp enantiomers (Figure 6D). The interactions between the chiral sensing interface and the amino acids dominate the chiral recognition specificity. The results show that the greater the steric hindrance, the more obvious the recognition effect.

Table 1 compares the sensor platform (CNT/PANI/SA/GCE) constructed in this article with the previous reports used to identify Trp enantiomers. The results show that the recognition ability of the sensing platform for Trp enantiomers is better than or equivalent to previous reports.[32–35]

3.5 | The optimization of experimental conditions and anti-interference ability

The incubation time between Trp isomers and CNT/PANI/SA/GCE was explored to optimize
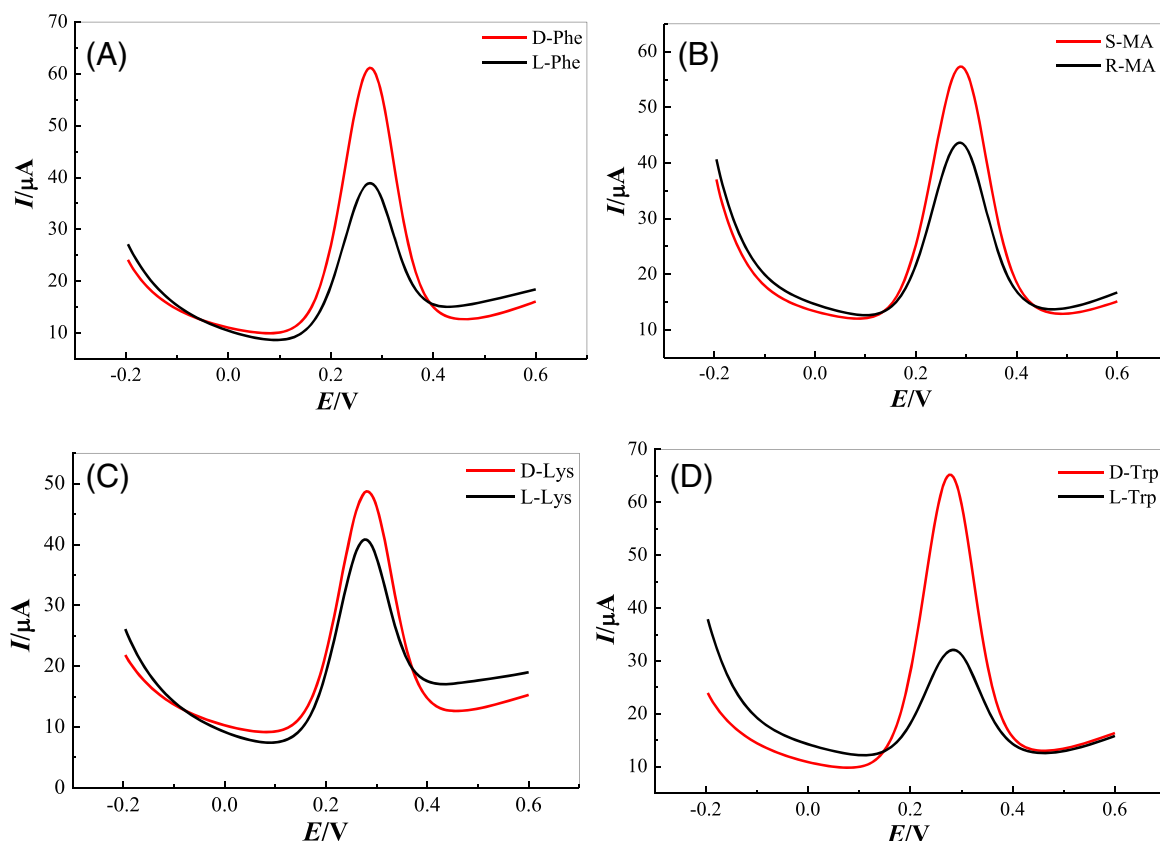
FIGURE 6 DPVs of 5-mM L-Phe and D-Phe (A), R-MA and S-MA (B), L-Lys and D-Lys (C), and L-Trp and D-Trp (D) interacted with CNT/PANI/SA/GCE

TABLE 1 Analytical performance of different modified electrodes for Trp enantiomers detection

Electrode substrate	Recognition mechanism	Method	Peak current ratio	Ref.
MWCNT-CS/GCE	Three-point interaction	DPV	-	Yu et al.[32]
β-CD-GNs/GCE	Three-point interaction	CV	2.05	Feng et al.[33]
NF/BPNSsG2-β-CD/GCE	Three-point interaction	SWV	1.49	Zou and Yu[34]
l-Cys/Au	Ligand exchange	CV	1.37	Chen et al.[35]
CNT/PANI/SA/GCE	Three-point interaction	DPV	2.1	This work

experimental conditions (Figure 7A). Peak currents of L-Trp and D-Trp reduce obviously from 10 to 25 s, and the optimal recognition effect is obtained the incubation time of 25 s. The peak currents gradually decline with increase of the incubation time 30 to 50 s, indicating the sites at sensing interface become oversaturated and lead to an unstable system.

Figure 7B shows that the recognition efficiency increased with an increase of the pH value of the recognized system solution from 4.5 to 5.5, but decreased when pH reach to 6.0. Therefore, the optimal pH of recognized system solution was selected as pH = 6.0. According to previous reports, the isoelectric point of Trp is 5.89.[2] The poor recognition efficiency in low pH system may be due

to SA is prone to be destroyed in strong acidic system, resulting in the volatility of the CNT/PANI/SA-based chiral interface. When pH is higher than isoelectric point (pH exceeded 6), Trp is negatively charged. The electrostatic repulsion between Trp isomers and negatively charged SA will prevent CNT/PANI/SA and L-Trp or D-Trp from interacting, thus leading to reduced recognition efficiency. These results indicate that the acid–base strength of the tested solution has significant influence on the recognition effect of chiral sensing interface.

As seen in Figure 7C, with an increase of the drop-coating volume from 3.0 to 8.0 μl, the peak current ratio increased. But when the dropcoating volume exceeds 8.0 μl, the peak current ratio decreased after 8.0 μl.
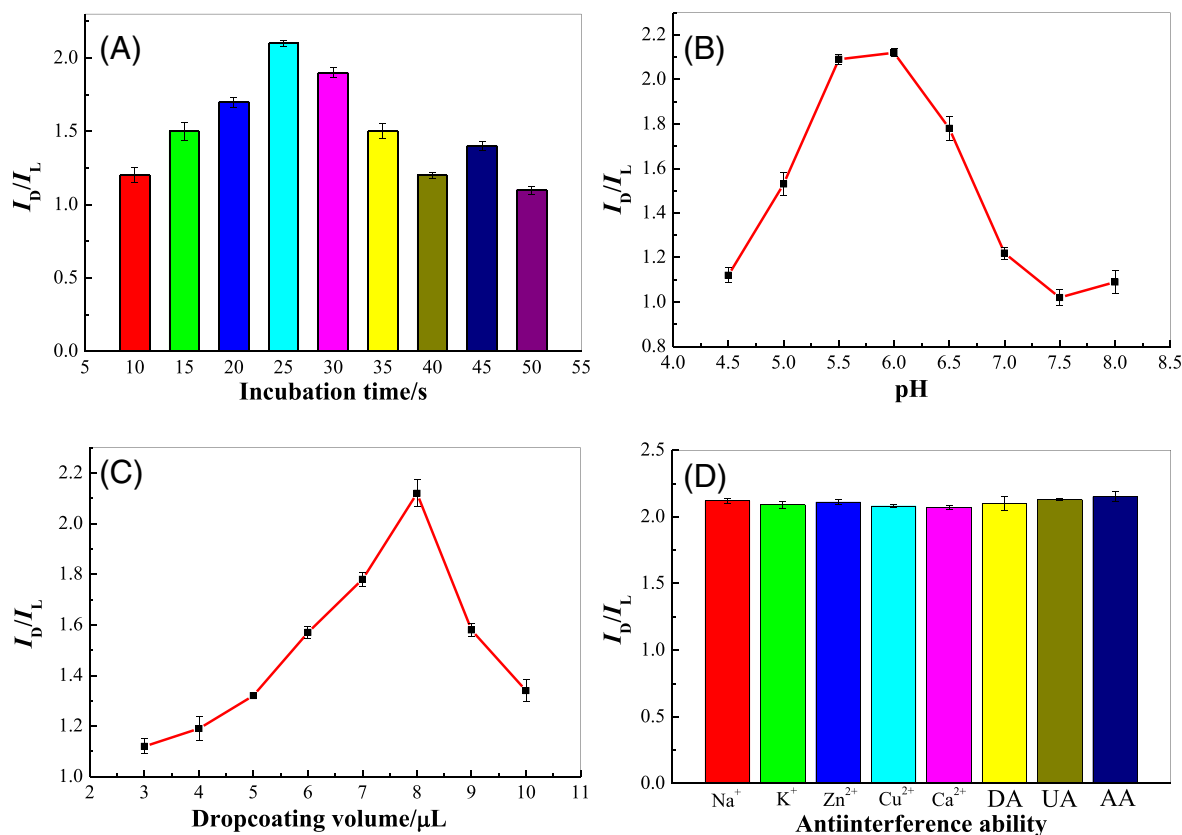
FIGURE 7 Optimization of the (A) incubation time, (B) pH, and (C) dropcoating volume of CNT/PANI/SA. (D) Investigation of the anti-interference ability of the chiral sensing platform based on the CNT/PANI/SA composite. The error bars are standard deviations of three parallel experiments

TABLE 2 Detection of L-Trp in actual samples ($n = 5$)

Sample	CL[a] (μM)	Added (μM)	Founded (μM)	RSD (%)	Recovery (%)
Human urine	1.8	0.5	2.22 ± 0.17	3.7	96.5
		1.0	2.91 ± 0.19	3.2	103.9
		10.0	12.1 ± 0.23	4.1	102.5
		50.0	51.6 ± 1.09	2.9	99.6
Human serum	2.7	0.5	3.15 ± 0.07	4.7	98.4
		1.0	3.61 ± 0.18	4.5	97.7
		10.0	13.2 ± 0.43	3.8	103.9
		50.0	53.4 ± 1.25	2.6	101.3

[a]Content of L-Trp in the actual sample.

Therefore, dropcoating volume of 8.0 μl was used as the optimal volume of CNT/PANI/SA. This result was attributable to synergy of CNT/PANI and SA: the excellent of electrical conductivity of CNT/PANI and the inherent chirality of SA. Before the optimal amount of CNT/PANI/SA, the peak current ratio between L-Trp and D-Trp can gradually increase with the increase of the dropcoating volume of CNT/PANI/SA. However,

excessive CNT/PANI/SA will hinder electron transmission with obviously declining identification signal recognition.

Considering the real application of the chiral sensing platform in the complex chiral recognition system, the anti-interference property also studied based on CNT/PANI/SA/GCE chiral sensing platform. Some potential interfering agents, such as metal ions with and

TABLE 3 Detection of D-Trp in actual samples ($n = 5$)

Sample	CD[a] (µM)	Added (µM)	Founded (µM)	RSD (%)	Recovery (%)
Human urine	3.1	0.5	3.72 ± 0.10	2.5	103.3
		1.0	4.07 ± 0.23	3.1	99.3
		10.0	13.3 ± 0.38	3.8	101.5
		50.0	53.9 ± 1.21	2.9	101.5
Human serum	0.0	0.5	0.48 ± 0.03	4.1	96.0
		1.0	1.02 ± 0.19	3.1	102
		10.0	9.7 ± 0.45	3.7	97
		50.0	49.4 ± 1.78	4.5	98.8

[a]Content of D-Trp in the actual sample.

without coordination ability, and biomolecules were introduced in recognized solution. As illustrated in Figure 7D, Na^+, K^+, Zn^{2+}, Cu^{2+}, Ca^{2+}, dopamine (DA), urea (UA), and ascorbic acid (AA) nearly had no effect on peak current ratio, indicating that the presence of interferences can be ignored. In general, the result showed that the CNT/PANI/SA-based chiral sensing interface possesses excellent anti-interference ability for the recognition of Trp enantiomers to interfering agent from complicated system.

3.6 | The application in real sample

To assess the practicability of the biosensors, the L-Trp and D-Trp of human urine and human serum real samples found via using standard addition methods. We can obtain from the experimental results analysis of real samples: for L-Trp (Table 2), the RSD range was from 2.6% to 4.7% and the recovery from 96.5% to 103.9%; for D-Trp (Table 3), the RSD change was from 2.5% to 4.5% and the recovery range from 96.0% to 103.3%. All these result showed the feasibility of the CNT/PANI/SA chiral biosensor in practical application.

4 | CONCLUSION

In summary, SA, CNT, and PANI were combined together via self-assembly for the fabrication of novel and effective chiral interfaces, which were used for the chiral recognition of Trp enantiomers through electrochemical measurement based on the synergetic properties of CNT/PANI and SA as well as different bonding affinity between CNT/PANI/SA with different targets. Compared with individual SA and CNT/PANI, the self-assembled CNT/PANI/SA nanocomposite demonstrated high stereoselectivity and excellent electrochemical property. The

stable CNT/PANI/SA-modified GCE presented an ingenious approach for recognizing Trp enantiomers. The proposed chiral sensing interface showed a good stability and high selectivity for L-Trp and D-Trp. This study is an example showed that self-assembled method can be used to synthesize chiral materials. The chiral sensing interface is successfully applied to detect L-Trp and D-Trp in an actual sample, which shows the potential application in chiral recognition.

DATA AVAILABILITY STATEMENT
The raw/processed data required to reproduce these findings cannot be shared at this time as the data also forms part of an ongoing study.

ORCID
Kunjie Wang https://orcid.org/0000-0003-3098-3776

REFERENCES
1. Thanzeel FY, Wolf C. Substrate-specific amino acid sensing using a molecular D/L-cysteine probe for comprehensive stereochemical analysis in aqueous solution. *Angew Chem.* 2017;56 (25):7276-7281.
2. Yu Y, Tao Y, Yang B, Wu D, Qin Y, Kong Y. Smart chiral sensing platform with alterable enantioselectivity. *Anal Chem.* 2017;89(23):12930-12937.
3. Ahn J, Ma S, Kim JY, et al. Chiral 2D organic inorganic hybrid perovskite with circular dichroism tunable over wide wavelength range. *J Am Chem Soc.* 2020;142(9):4206-4212.
4. Liu Z, Ai J, Kumar P, et al. Enantiomeric discrimination by surface-enhanced Raman scattering-chiral anisotropy of chiral

nanostructured gold films. *Angew Chem*. 2020;132(35): 15338-15343.

5. Han Y, Lv W, Chen H, et al. Chiral fluorescent silicon nanoparticles for aminopropanol enantiomer: fluorescence discrimination and mechanism identification. *Anal Chem*. 2020; 92(5):3949-3957.

6. Zou J, Lan XW, Zhao GQ, Huang ZN, Liu YP, Yu JG. Immobilization of 6-*O*-α-maltosyl-β-cyclodextrin on the surface of black phosphorus nanosheets for selective chiral recognition of tyrosine enantiomers. *Microchim Acta*. 2020;187(11):1-11.

7. Zou J, Yu JG. Chiral recognition of tyrosine enantiomers on a novel bis-aminosaccharides composite modified glassy carbon electrode. *Anal Chim Acta*. 2019;1088:35-44.

8. Zou J, Chen XQ, Zhao GQ, Jiang XY, Jiao FP, Yu JG. A novel electrochemical chiral interface based on the synergistic effect of polysaccharides for the recognition of tyrosine enantiomers. *Talanta*. 2019;195:628-637.

9. Wu D, Pan F, Gao L, Tao Y, Kong Y. An ionic-based carbon dot for enantioselective discrimination of nonaromatic amino alcohols. *Analyst*. 2020;145(9):3395-3400.

10. Wu S, Ye Q, Wu D, Tao Y, Kong Y. Enantioselective recognition of chiral tryptophan with achiral glycine through the strategy of chirality transfer. *Anal Chem*. 2020;92(17):11927-11934.

11. Wu D, Pan F, Gao L, Tao Y, Kong Y. Enantioselective limiting transport into a fixed cavity via supramolecular interaction for the chiral electroanalysis of amino acids regardless of electroactive units. *Anal Chem*. 2020;92(20):13711-13717.

12. Guo J, Wei X, Lian H, Li L, Sun X, Liu B. Urchin-like chiral metal-organic framework/reduced graphene oxide nanocomposite for enantioselective discrimination of D/L-tryptophan. *ACS Appl Energ Mater*. 2020;3(4):3675-3683.

13. Kotake M, Sakan T, Nakamura N, Senoh S. Resolution into optical isomers of some amino acids by paper chromatography. *J Am Chem Soc*. 1951;73(6):2973-2974.

14. Chankvetadze B. Recent trends in preparation, investigation and application of polysaccharide-based chiral stationary phases for separation of enantiomers in high-performance liquid chromatography. *Trends Anal Chem*. 2020;122:115709.

15. Niu X, Yang X, Mo Z, et al. Fabrication of an electrochemical chiral sensor via an integrated polysaccharides/3D nitrogen-doped graphene-CNT frame. *Bioelectrochemistry*. 2020;131: 107396.

16. Bao L, Dai J, Yang L, et al. Electrochemical recognition of tyrosine enantiomers based on chiral ligand exchange with sodium alginate as the chiral selector. *J Electrochem Soc*. 2015;162(7): H486-H491.

17. Niu X, Yang X, Mo Z, et al. Voltammetric enantiomeric differentiation of tryptophan by using multiwalled carbon nanotubes functionalized with ferrocene and β-cyclodextrin. *Electrochim Acta*. 2019;297:650-659.

18. Niu X, Yang X, Mo Z, et al. Electrochemical chiral sensing of tryptophan enantiomers by using 3D nitrogen-doped reduced graphene oxide and self-assembled polysaccharides. *Microchim Acta*. 2019;186(8):557.

19. Yang X, Niu X, Mo Z, et al. Perylene-functionalized graphene sheets modified with chitosan for voltammetric discrimination of tryptophan enantiomers. *Microchim Acta*. 2019;186(6):333.

20. Yuk H, Lu B, Lin S, et al. 3D printing of conducting polymers. *Nat Commun*. 2020;11(1):1-8.

21. Zhou C, Ren Y, Han J, Xu Q, Guo R. Chiral polyaniline hollow nanotwists toward efficient enantioselective separation of amino acids. *ACS Nano*. 2019;13(3):3534-3544.

22. Wu X, Tang L, Zheng S, et al. Hierarchical unidirectional graphene aerogel/polyaniline composite for high performance supercapacitors. *J Power Sources*. 2018;397:189-195.

23. Abdulla S, Mathew TL, Pullithadathil B. Highly sensitive, room temperature gas sensor based on polyaniline-multiwalled carbon nanotubes (PANI/MWCNTs) nanocomposite for trace-level ammonia detection. *Sensor Actuat B*. 2015;221:1523-1534.

24. Yan Y, Cheng Q, Wang G, Li C. Growth of polyaniline nanowhiskers on mesoporous carbon for supercapacitor application. *J Power Sources*. 2011;196(18):7835-7840.

25. Zhang Z, Wei Z, Wan M. Nanostructures of polyaniline doped with inorganic acids. *Macromolecules*. 2002;35(15):5937-5942.

26. Monkman AP, Adams P. Optical and electronic properties of stretch-oriented solution-cast polyaniline films. *Synth Met*. 1991;40(1):87-96.

27. Zengin H, Zhou W, Jin J, et al. Carbon nanotube doped polyaniline. *Adv Mater*. 2002;14(20):1480-1483.

28. Yan J, Wei T, Fan Z, et al. Preparation of graphene nanosheet/carbon nanotube/polyaniline composite as electrode material for supercapacitors. *J Power Sources*. 2010;195(9): 3041-3045.

29. Wang YG, Li HQ, Xia YY. Ordered whiskerlike polyaniline grown on the surface of mesoporous carbon and its electrochemical capacitance performance. *Adv Mater*. 2006;18(19): 2619-2623.

30. Wu D, Kong Y. Dynamic interaction between host and guest for enantioselective recognition: application of β-cyclodextrin-based charged catenane as electrochemical probe. *Anal Chem*. 2019;91(9):5961-5967.

31. Benesi HA, Hildebrand JHJ. A spectrophotometric investigation of the interaction of iodine with aromatic hydrocarbons. *J Am Chem Soc*. 1949;71(8):2703-2707.

32. Yu LY, Liu Q, Wu XW, Jiang XY, Yu JG, Chen XQ. Chiral electrochemical recognition of tryptophan enantiomers at a multi-walled carbon nanotube-chitosan composite modified glassy carbon electrode. *RSC Adv*. 2015;5(119):98020-98025.

33. Feng W, Liu C, Lu S, Zhang C, Zhu X, Liang Y. Electrochemical chiral recognition of tryptophan using a glassy carbon electrode modified with β-cyclodextrin and grapheme. *Microchim Acta*. 2014;181(5-6):501-509.

34. Zou J, Yu JG. Nafion-stabilized black phosphorus nanosheets-maltosyl-β-cyclodextrin as a chiral sensor for tryptophan enantiomers. *Mater Sci Eng C*. 2020;112:110910.

35. Chen Q, Zhou J, Han Q, Wang Y, Fu Y. Electrochemical enantioselective recognition of tryptophane enantiomers based on chiral ligand exchange. *Colloid Surface B*. 2012;92:130-135.